Effects of non-isotropic blockage on a tidal turbine modeled with the Actuator-Line method

Enzo Mascrier, Federico Zilic de Arcos, Grégory Pinon

Effects of non-isotropic blockage on a tidal turbine modeled with the Actuator-Line method

Enzo Mascrier, Federico Zilic de Arcos, Grégory Pinon

Abstract—**This paper presents a study on the effects of non-isotropic blockage on a tidal turbine using numerical simulations. A tidal rotor was modeled with OpenFOAM using the Actuator-Line method under four different blockage ratios, four different aspect ratios, and four different tip-speed ratios. The study analyzes the blade-boundary interactions through observations on the rotor integrated loads and power, sectional forces, local angles of attack, and turbine wake characteristics. The simulations reveal that, while reducing aspect ratios (i.e., bringing the boundaries closer to the rotor) has a negative impact on performance at low blockage, increasing blockage reduces the influence of aspect ratio on time-averaged thrust and power. However, the changes in aspect ratio can result in significant thrust and power fluctuations in time, especially at blade sections close to the tip. On a local scale, the impact of aspect ratio is observed on angles of attack changes due to flow acceleration, especially close to the blade tip. The effects of blockage and aspect ratio can also be observed in the development of the turbine wake. The presence of boundaries limits the expansion of the wake and its interaction with the surrounding velocity field, affecting wake recovery.**

Index Terms—**Tidal Energy, Anisotropic Blockage, Actuator Line, CFD**

I. Introduction

THE discussion of blockage effects on rotors emerged during the development of wind tunnel testing [3, 6, 7]. Those wind tunnels played a significant role in the experimental testing of airfoils and turbine blades. In its simplest form, blockage refers to the interaction between a body, in this case a rotor, and the outer boundaries of a tunnel. Blockage is normally characterized by the ratio of the rotor swept area to the channel cross-sectional area, and is denoted here by β. Blockage effects can lead to changes in performance and wake development of a turbine [2].

Previous studies have shown that increasing blockage can enhance the performance of turbines. Garrett and Cummins [5] established that the maximum power coefficient C_P is superior to the Betz limit by a factor of $(1-\beta)^{-2}$. Increasing the maximum power corresponds to higher energy yields and reduced costs. However, as the maximum power increases, the thrust experienced by the turbine is likely to increase as well. This results in a higher load on the turbine, leading to accelerated degradation

To characterize and remove blockage effects on the power and thrust of a rotor operating in blocked-flow environments, correction methods have been developed [1, 10, 14]. However, such corrections are only developed for isotropic blockage conditions. This term, isotropic blockage, is used in literature to describe the blockage that occurs uniformly in all directions. However, studies on anisotropic blockage, which occurs in specific directions, are limited [9].

The interaction of turbine blades with their surrounding boundaries, in the case of anisotropic blockage, can significantly affect the performance of the turbine. As blades rotate, they interact with the surrounding environment. This interaction can cause disturbances in the velocity and pressure fields, leading to variations in angles of attack and, thus, local forces. Therefore, understanding the impact of blade-boundary interaction on turbine loads and performance, especially in the context of non-isotropic blockage, is crucial for the development of more efficient and reliable tidal turbines.

This study aims to investigate the impact of anisotropic blockage on the performance of a tidal turbine. A 20 m diameter rotor was modeled in OpenFOAM, an open-source CFD software, using the Actuator Line method [21]. This method models rotor blades replacing them in a fluid simulation with collections of points arranged in lines. The collocation points move in time to mimic the rotation of the blade, and each time-step body forces are calculated and applied to the flow. These forces are calculated using Blade-Element Theory (BET), using tabulated lift and drag coefficients and the sampled flow around each collocation point. This method avoids modeling the blade walls and therefore reduces the computational cost. The actuator line method has been validated successfully over the past few years [15, 20].

The first objective of this study is to characterize isotropic blockage effects to define a set of benchmark conditions. The data obtained from this part will serve as a reference for the subsequent study of anisotropic blockage. The ultimate objective of our study is to determine the influence of anisotropic blockage compared with the isotropic case. Several parameters such as power, thrust, angles of attack, in addition to observations on the flow around the rotor and wake, are

E. Mascrier is with the Science department at the University Le Havre Normandie (e-mail: enzo.mascrier@etu.univ-lehavre.fr)

F. Zilic de Arcos and G. Pinon are with the Laboratoire Ondes et Milieux Complexes, UMR 6294 CNRS, Université Le Havre Normandie (e-mail: federico.zilic@univ-lehavre.fr / gregory.pinon@univ-lehavre.fr)

Digital Object Identifier:
https://doi.org/10.36688/ewtec-2023-348

used in our analysis.

II. Methods

A. Study parameters

The turbine simulated in this study is the Sch15B, a tidal rotor designed by Schluntz and Willden [18]. It is a three-bladed 20-meter diameter rotor, and it is specifically designed to operate under a blockage ratio of 19.7 %. The blade consists of a single RISØ-A1 24 airfoil [4] from 25% of the blade radius up to the tip.

In our study, the turbine was placed within a rectangular domain that is 15 rotor diameters in length. The rotor is placed at the center of the channel and at a $5D$ distance from the inlet. The channel's width and height are dependent upon the imposed blockage and aspect ratio. The blockage (β) and the aspect ratio (AR) are defined as :

$$\beta = \frac{A_{rotor}}{A_{channel}} \tag{1}$$

$$AR = \frac{H}{w} \tag{2}$$

with A_{rotor} the swept area of the rotor, $A_{channel}$ the cross-sectional area of the channel, w and H the respective width and height of the channel.

Four distinct blockage ($\beta \in$ [1 %, 5 %, 10%, 19.7 %]) and aspect ratios (AR $\in$ [0.3, 0.5, 0.75, 1]) were considered. We excluded the potential influence of a fixed structure or nacelle on the simulations. The simplified channel geometries of our study intends to provide a closer approximation to real tidal channels with complex bathymetries, compared to isotropic blockage cases, while still allowing the detailed study of the relevant hydrodynamics.

The rotor was simulated at different tip-speed ratios (TSR) λ:

$$\lambda = \frac{\omega R}{V_\infty} \tag{3}$$

with ω the angular velocity of the turbine ($m.s^{-1}$) and R the radius of the rotor (m).

Four tip-speed ratios ($\lambda \in$ [4.0, 5.0, 6.0, 7.0]) were considered for each different case of blockage and aspect ratio through variations in the turbine's rotational speed. The current speed was kept constant at 3 $m.s^{-1}$ for all analyzed cases.

Overall, the study consists of 64 simulations, where each case is uniquely identified by a set of β, AR, λ.

B. CFD Model

Simulations were conducted using a Reynolds-Averaged Navier Stokes (RANS) computational fluid dynamics (CFD) model within OpenFOAM v2012. The $k-\omega$ SST turbulence closure model [12] was selected with the updated coefficients of Menter et al. [13]. The turbulence kinetic energy k and the specific turbulence dissipation ω are imposed as a fixed value at the inlet of the channel. The turbulence intensity T_i and the turbulent length scale l_T are respectively set to 8.3 % and 2.35 m. A velocity inlet and a pressure outlet are imposed while a slip condition is enforced on the remaining boundaries of the domain.

We used the PIMPLE algorithm for our calculations, a hybrid of the PISO and SIMPLE algorithms. It is a time-stepping algorithm that solves the Navier-Stokes equations for incompressible flow. Computation steps are combined with correction steps until the convergence of the solution. A second-order linear Gaussian was used as a discretisation scheme.

C. Actuator Line Method

The Actuator Line Method (ALM) was first developed in the early 2000s for modeling the wake of wind turbines. This method offers the advantage of significantly reducing computational costs by representing the turbine blades as lines composed of points where body forces are applied to mimic the effect of the rotor on the flow, as represented in Fig 1.

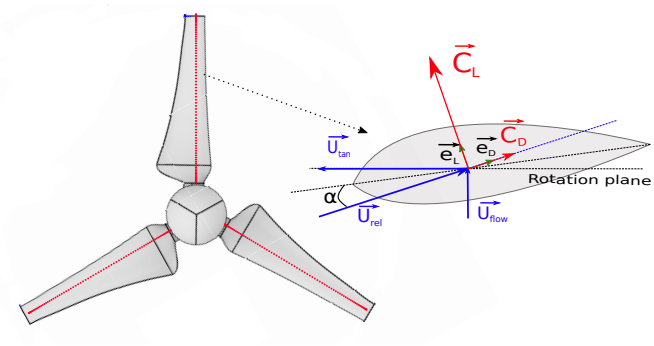

Fig. 1. Airfoil section with applied forces. Collocations points are represented by red points.

This approach eliminates the need to create a complex mesh around the blades, thus avoiding the computational expense of resolving the blade walls and their boundary layer. To calculate the body force, the blade-element approach is employed, which involves calculating the forces using tabulated drag and lift coefficients C_D and C_L, alongside the local angle of attack α. The lift and drag forces are then used to determine the aerodynamic force per unit length, defined as follows:

$$d\mathbf{F} = \frac{1}{2}\rho c \mathbf{U}_{rel}^2 (C_L \mathbf{e}_L + C_D \mathbf{e}_D) dr \tag{4}$$

where ρ is the density of water ($kg.m^{-3}$), c the chord of the blade (m). e_L and e_D are unitary vectors that carries respectively the lift and the drag vectors. $\mathbf{U}_{rel}$ represents the relative velocity at the blade section ($m.s^{-1}$). It reads as :

$$\mathbf{U}_{rel}^2 = \mathbf{U}_{flow}^2 + \mathbf{U}_{tan}^2 \tag{5}$$

with $\mathbf{U}_{flow}$ the velocity of the income flow and $\mathbf{U}_{tan}$ the tangential velocity of the blade element. The $\mathbf{U}_{rel}$ vector includes the blade's axial and tangential inductions. It is sampled directly from the flow around the collocation point using the line-average method of Jost et al. [8]. This is a robust flow-sampling method implemented within the AL model by Zormpa et al. [23].

In the present case, the distance between each blade element is not constant. The actuator points are distributed more densely at the root and tip of the turbine following a cosine distribution.

D. Mesh study

In order to investigate the discretization effects on the accuracy and efficiency of the numerical simulations, a mesh convergence study was conducted. Three different meshes were simulated: fine, medium, and coarse (respectively named 1, 2, and 3). Simulations are performed under a high tip-speed ratio value (λ = 7) and with an isotropic blockage β of 1 %. Rotor positioning is the same as described in section II-A. The overall mesh comprises of a large numbers of hexahedral cells, making the simulations computationally intensive. The simulations were performed on 6 nodes with 160 cores on the MYRIA Cluster at the Centre Régional Informatique et d'Applications Numériques de Normandie (CRIANN). Each case requires a time duration of approximately nine hours to complete.

The grid-convergence index (GCI), a method first introduced by Roache [17], was used to evaluate the error introduced by numerical discretisation in our simulations. The GCI is used to estimate the error reduction when refining the grid size in a simulation. The main objective is to quantify the error between two meshes by progressively increasing the mesh resolution and thus, estimate the convergence of the solution. The grid-convergence index (GCI) is defined as follows:

$$GCI_{i+1,i} = \frac{F_s|e_{i+1,i}|}{r_{i+1,i}^p - 1} \tag{6}$$

with F_s a safety factor, $e_{i+1,i}$ the error between two meshes ($e_{i+1,i}$ = e_{i+1} - e_i), $r_{i+1,i}$ is the mesh refinement ratio ($r_{i+1,i}$ = $(N_{i+1}/N_i)^{\frac{1}{2}}$). N is the number of cells in the simulation. r is constant in this study, so the order of convergence p is defined as:

$$p = \frac{ln(\frac{f_3 - f_2}{f_2 - f_1})}{ln(r)} \tag{7}$$

with f_i a solution obtained with the mesh i. The variable f_i will be either C_T or C_P from Eq. 9 and 10. In addition, we employed the relative error E_R, i between two successive refinement stages, which is defined as :

$$E_R, i = \frac{f_i - f_{i-1}}{f_i} \tag{8}$$

Following the recommendations of Roache [17] when 3 meshes are compared, a safety factor F_s of 1.25 was used.

Two variables were used for assessing mesh convergence: the integrated thrust and power coefficients, which are defined as:

$$C_T = \frac{T}{0.5\rho A_{rotor} V_\infty^2} \tag{9}$$

$$C_P = \frac{P}{0.5\rho A_{rotor} V_\infty^3} \tag{10}$$

with T the integrated thrust (N), P the integrated power (W), ρ the density of water ($kg.m^{-3}$), A_{rotor} the swept area of the turbine (m^2) and V_∞ the velocity of the undisturbed incoming flow ($m.s^{-1}$). The obtained simulation values are summarized in Table I.

Thrust coefficient C_T

N	f (-)	E_R (%)	e (-)	GCI (%)
0.885 M	1.2033	-	-	-
6.947 M	1.1855	-1.501	-0.0178	0.1055
56.099 M	1.18635	0.068	0.0008	0.0048

Power coefficient C_P

N	f (-)	E_R (%)	e (-)	GCI (%)
0.885 M	0.4417	-	-	-
6.947 M	0.4278	-3.252	-0.0139	0.0825
56.099 M	0.42895	0.275	0.0012	0.0067

TABLE I
MESH ANALYSIS STUDY

With a mesh refinement ratio of 2.8, the order of convergence is determined to be third order, as per Eq. 7. Based on the results presented in Table I, it can be observed that the maximum relative error between the medium and fine meshes is 0.068 % and the Grid-Convergence Index is calculated to be 0.0048 % for the thrust coefficient. Regarding the power coefficient, the GCI is equal to 0.0067 % and the error is 0.275 % between the medium and the fine mesh. These differences are small for the purposes of this work, and the medium mesh, with 130 cells over the rotor diameter ($2R/\Delta X$ = 130) is deemed appropriate for the development of our study. Simulations conducted using the medium mesh require less computational power and can be completed within approximately 9 hours compared to the 16 hours and a half required for the fine mesh running on the aforementioned cluster.

III. RESULTS AND DISCUSSION

1) Integrated power and Thrust analysis: In Fig. 2, power and thrust coefficients are plotted as a function of the TSR.

Markers represent the simulated results extracted during the post-processing and dotted lines that correspond to cubic splines are provided for reference. In this case, the results correspond to the aspect ratio of 1, the isotropic blockage condition.

Fig. 2 shows results that agree with the general trends described in the literature [16]: blockage increases the rotor power and thrust. The difference between β = 0.01 and β = 0.05 is small, with an average difference of 1.8 % for power coefficients and 0.9 % for the thrust coefficients. The variation becomes significant for higher blockage ratios, with a difference of 12.5 % for the maximum power between β = 0.05 and β = 0.197. A shift on the maximum C_P peak towards higher λ is also observed when the global blockage increases, in agreement with previous observations made by Wimshurst and Willden [22]. For β = 0.01, the maximum C_P occurs at λ = 4.895, and it moves to λ = 5.637 when β = 0.197.

The impact of the non-isotropic blockage is shown in Fig. 3 for the integrated power and thrust. For clarity, only two different values of blockage and four values of the aspect ratio are plotted as a function of the TSR.

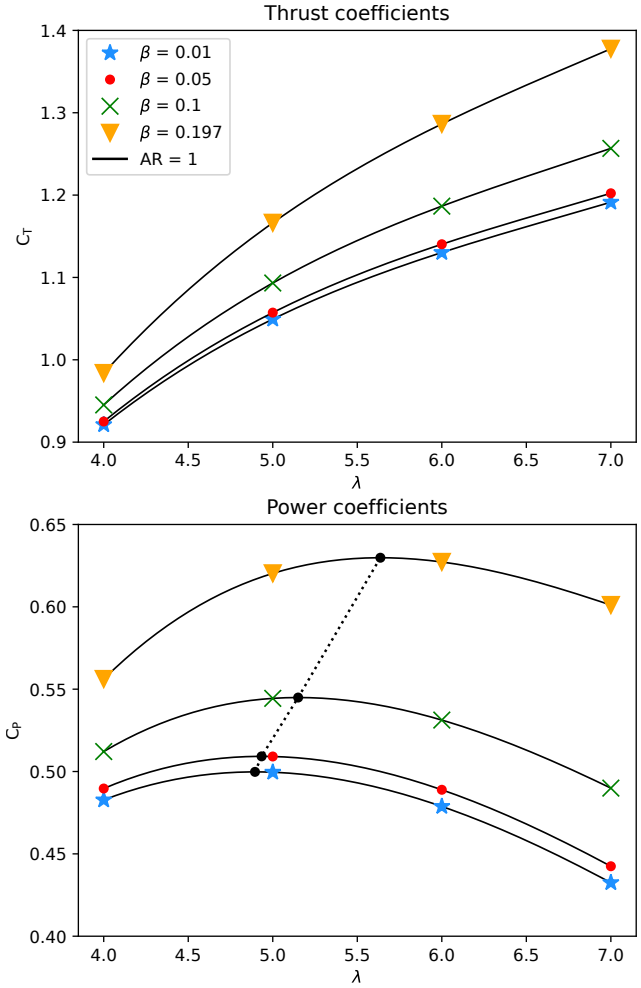

Fig. 2. Integrated thrust (top) and power (bottom) coefficient for different isotropic blockage. The dash line and black dots represents the position of the maximum at each blockage.

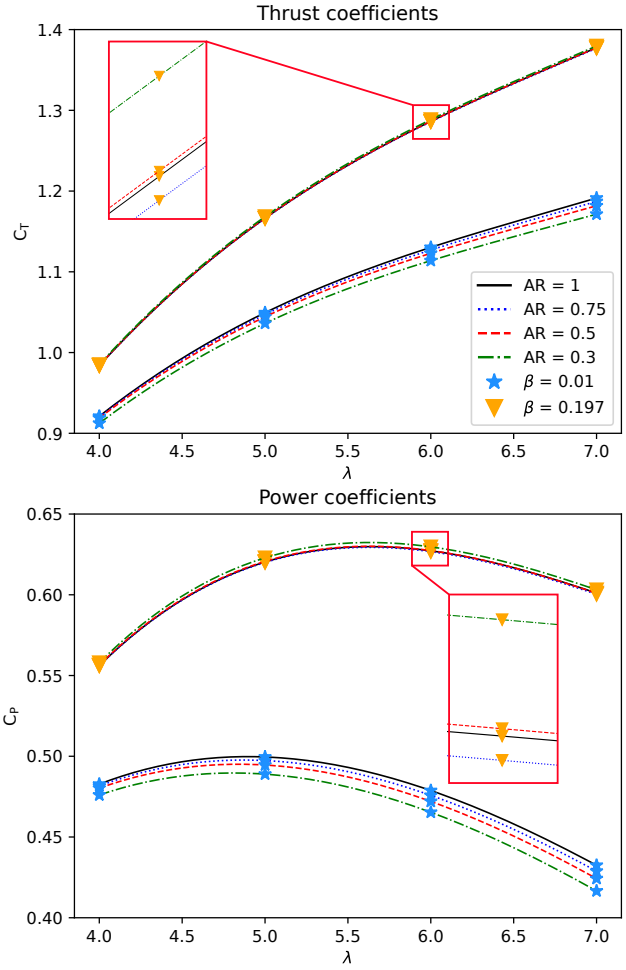

Fig. 3. Influence of the aspect ratio on integrated thrust and power coefficients for two blockage values.

The results show two different trends. For the lowest blockage value (β = 0.01), the aspect ratio tends to reduce the turbine's power and thrust by maximum differences of 2.13 % and 1.26 %, respectively, comparing the isotropic case with the lowest aspect ratio. For $\beta \geq 0.05$, the aspect ratio shows only a modest impact on thrust and power. This difference reaches a maximum of 0.43 %, comparing maximum C_p, for the 19.7 % blockage case. However, for an aspect ratio of 0.3, a slight increase in power can be observed for all TSR values, while for an AR of 0.75, a small decrease is observed compared to the isotropic case. These opposite changes are small but below the numerical discretisation error.

2) Axial force: Axial force distributions along blades were analyzed. Fig. 4 shows the axial force for each TSR simulated. The continuous line represents the time-averaged force at different blade sections, while the shaded regions represent the fluctuating force range (mean value plus/minus two standard deviations).

The time-averaged forces, for a fixed blockage, show a maximum value that is almost constant regardless of aspect ratio. At λ = 7, a difference of 1.75 % is observed between β = 0.01 and 0.18 % when the blockage is equal to 0.197.

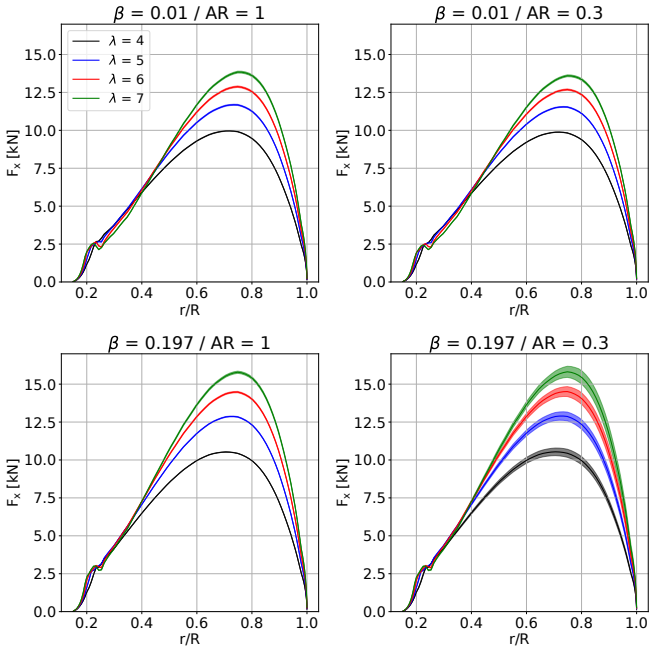

Fig. 4. Time-averaged spanwise axial force distribution for two blockage and aspect ratio values

For the blockage value of 0.01, negligible load fluctuations are observed. However, the cases with high blockage and low AR show larger load fluctuations

concentrated at approximately $0.6 \leq r/R \leq 0.9$, as shown in Fig. 4. These correspond to local fluctuations of up to $\pm$ 2.62 % of the mean. In such conditions, load variations will alter the behavior of the turbine. Over the long term, load fluctuations have the potential to damage the turbine and increase the risk of premature failure [11].

For the high blockage cases, the mean axial force is the same at each r/R value, regardless the AR. But as the AR decreases, time fluctuations increase.

3) Angle of Attack: To explain the influence of the boundaries, the spanwise distributions of angles of attack were examined. Variation can be observed in Fig. 5. The four analyzed blockage ratios are presented for two different aspect ratios (1 and 0.3) and at a representative $\lambda = 5.0$. The values are averaged over 10 blade rotations.

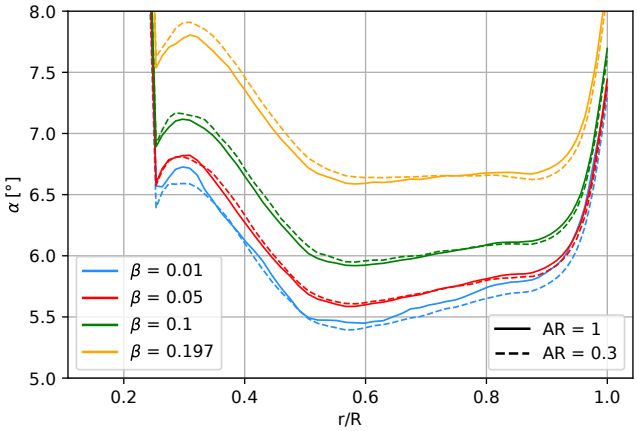

Fig. 5. Angle of attack along the spanwise at a tip-speed ratio λ = 5. Two aspect ratios are compared for different blockage values.

The results show that an increase in blockage results in a step-increase in angles of attack across the span of the blade.

For $\beta = 0.01$, the angles of attack along the entire blade show a modest reduction at the lowest AR. This is related to the observations in section III-1. In particular, according to Blade-Element Theory, the sectional thrust coefficient is defined as :

$$C_X = C_L \cos(\phi) + C_D \sin(\phi), \tag{11}$$

where ϕ is the inflow angle relative to the rotor plane. For a typical rotor operating under near-optimal conditions, the drag coefficient and $\sin\phi$ are small and, thus, the second term in the equation above is negligible. Furthermore, $\cos(\phi) \approx 1$ and, thus, Eq. 11 can be approximated as:

$$C_X \approx C_L \tag{12}$$

In the pre-stall range, the lift coefficient is approximately proportional to the angle of attack. It follows that:

$$C_X \propto \alpha \tag{13}$$

Consequently, the lower angles of attack across the blade, for $\beta = 0.01$ and non-isotropic aspect ratios, lead to a lower integrated thrust, as observed in section III-1. Sectional tangential force coefficients are less straightforward to analyse, since drag and inflow angle play a non-negligible role. However, for the range of analysed cases, the same trends are observed for C_P and C_T.

For blockages larger than 1%, the non-isotropic cases show a different trend. Similar to the low blockage case, the outer sections of the blade show a modest reduction in mean angles of attack for lower aspect ratios. However, the lower AR cases also show increased mean angles of attack across inner sections of the blade. The point where the isotropic and non-isotropic angles of attack intersect, i.e., the transition from higher to lower α, move further outboard as blockage increases.

The two opposite effects of AR on angles of attack along the blade, for cases where $0.05 \leq \beta \leq 0.197$, are the cause for the different trends observed in section III-1. Increased angles of attack typically lead to higher local thrust and power, while lower angles of attack have the opposite effect. The balance across the blade and the cancellation of these two effects with lower aspect ratios result in a limited impact of AR on time-averaged C_P and C_T. The varying position of the intersect between the α curves for different blockage and aspect ratios define whether a small increase or reduction in power and thrust are produced, as shown in fig. III-1.

Fig. 6 represents the time-averaged angle of attack variation along the span for a fixed blockage of 0.197 and aspect ratios of 1 and 0.3. The solid and the dashed line represent the mean value at each location obtained during the final 10 rotational periods. The shaded region characterizes the fluctuations of the angle of attack in time through the time-averaged values plus/minus two standard deviations.

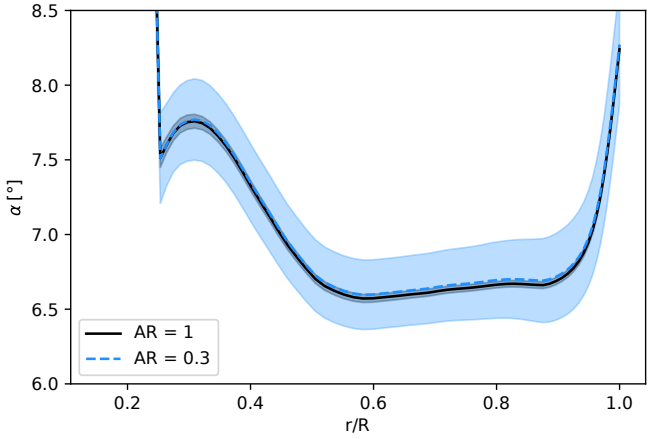

Fig. 6. Time averaged angle of attack along the spanwise at at β = 0.197 and λ = 5. Lines represent the average values and filled parts represent time fluctuations.

As before, the mean values are similar between the two cases. However, the figure shows how angle of attack fluctuations increase with aspect ratio across the entire span of the blade. The relative range of variability in the angle of attack is comparable to that observed for the thrust, as reflected by Eq. 13.

Since fluctuations in angles of attack are not shown by the time-averaged values, changes in thrust and power coefficients are not significantly noticeable.

However, the fluctuations shown in Fig. 6 also highlights that aspect ratio contributes to variations in the

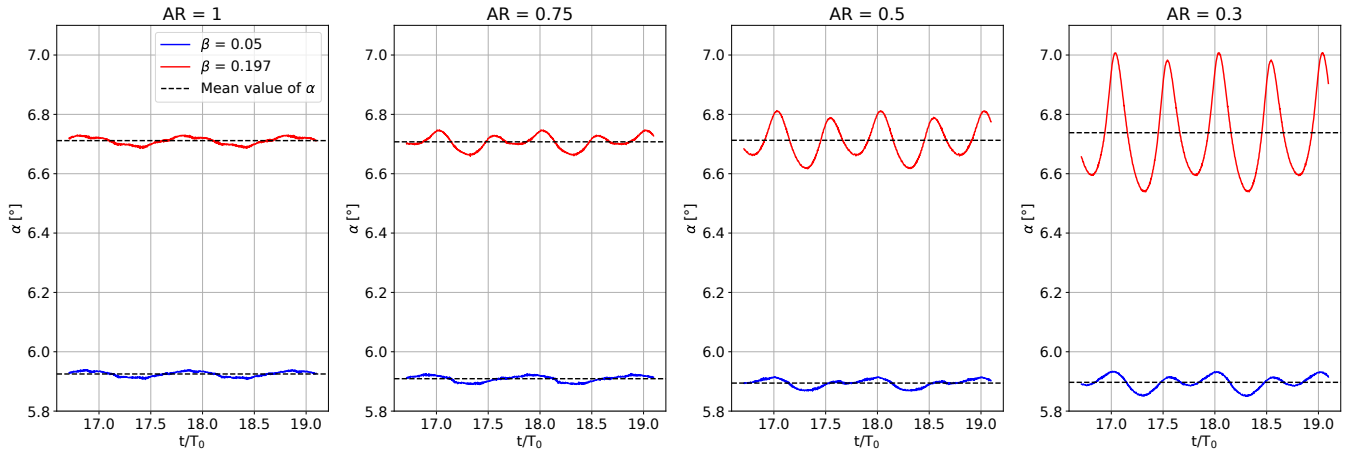

Fig. 7. Time-normalized variation of angle of attack at a radial location r/R = 0.9 and a tip-speed ratio λ = 5.

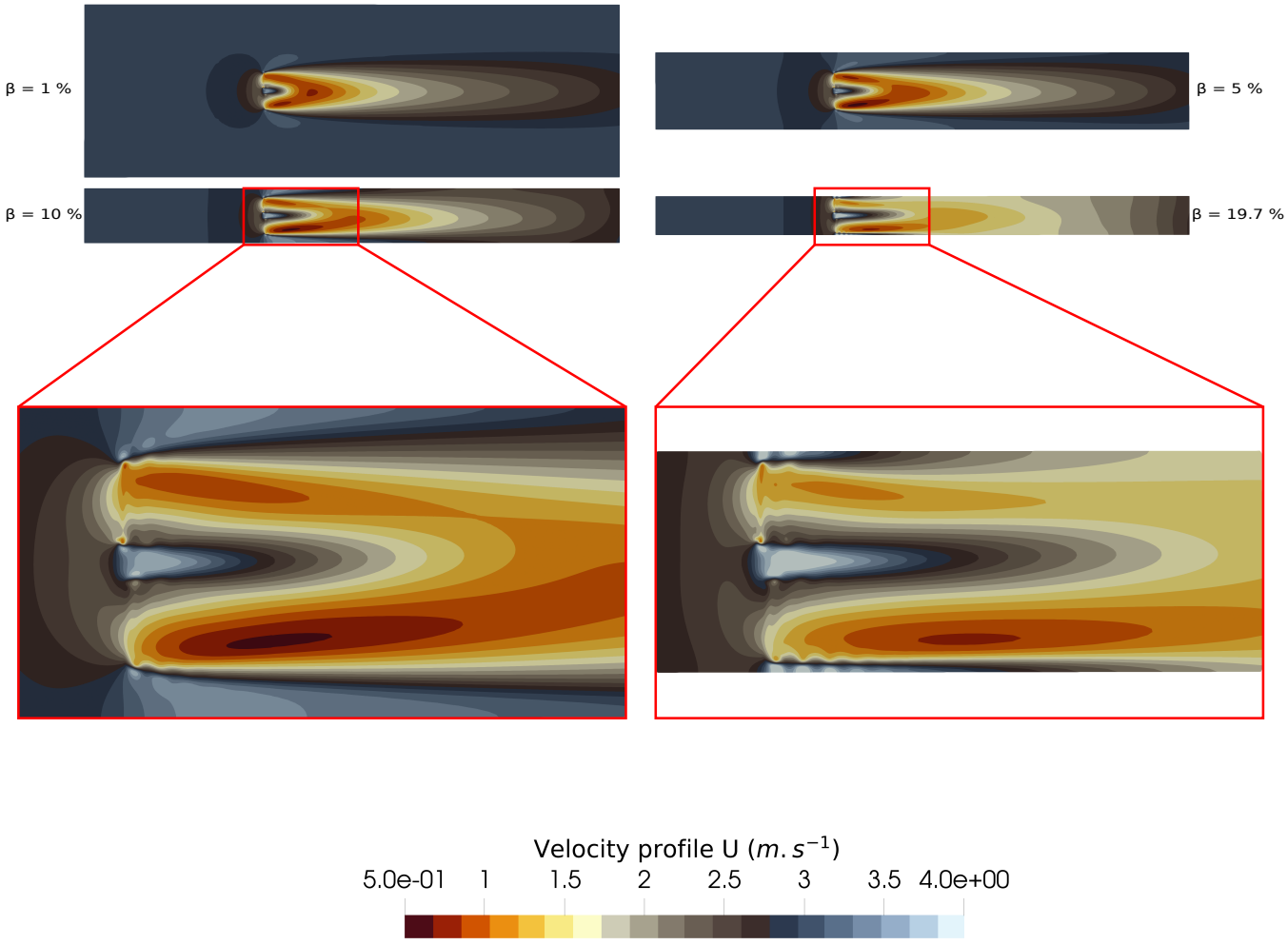

Fig. 8. Visualization of the velocity profile at an aspect ratio of 0.3 for different blockages. High hydrodynamics conditions are imposed (λ = 7) to facilitate the visualization.

angle of attack and, thus, in load fluctuations of similar magnitude.

Increasing the blockage and changing the aspect ratio constraints the flow around the turbine. To investigate this phenomenon, the angle of attack at $r/R = 0.9$ as a function of time and normalized by rotational period is plotted in Fig. 7. T_0 represents the turbine's rotation period.

As previously observed, the mean angles of attack remain relatively constant across all aspect ratios. For $\beta = 0.05$, small quasi-sinusoidal variations are observed when the aspect ratio is greater or equal to 0.75. For the AR of 0.5 and 0.3, boundaries are closer and that impact is visible: at the beginning of one period, as the blade approaches the top dead center, the flow velocity around the blade increases due to the flow acceleration at the bypass between the rotor and the upper boundary, inducing the peak angle of attack

observed. At $t/T_0 \approx 17.25$, the blade is now far from the boundaries, so the bypass flow effects are minimized and, thus, the angle of attack decreases. At half of its rotation, the blade is close again to the boundary, therefore, the blade is in the same state as T = 0 but in the opposite direction.

For β = 0.197, the phenomenon becomes more significant. For the aspect ratio of 0.3, the angle of attack varies by 0.45 ° depending on the position of the blade while it is only 0.08 ° for the 5 % blockage. More pronounced effects are observed at a lower aspect ratio. This is attributed to the shorter distance from the blade tip to the boundary for the higher blockage case.

The observed decrease in the angle of attack can be interpreted as a reduction in the velocity surrounding the blade. The velocity distribution in the channel is impacted by the aspect ratio. An analysis of the velocity profile is presented to provide confirmation of this effect.

Fig. 8. represents a side view of the velocity profile around the turbine for four blockage ratios at λ = 7 and for an aspect ratio of 0.3. The chosen TSR is specifically considered due to the increased significance of hydrodynamic conditions, resulting in more pronounced effects on the wake.

The velocity profiles confirm our previous observations: the flow undergoes an acceleration at the tip and at the center as blockage increases. The current initial velocity is increased by 34 % at the tip of the blade, when the aspect ratio is 0.3, affecting wake development. This is discussed in section III-5.

The velocity distribution around the blades exhibits a resemblance to the outcomes demonstrated in Fig. 5. The variation in the angle of attack can be attributed to the complex velocity profile resulting from the interaction between the fluid flow, the blade, and the boundary. The hypothesis mentioned on the time variation of the angle of attack is now confirmed based on the obtained results: a decrease in the aspect ratio leads to a flow acceleration on the outboard sections of the blade and the bypass between the rotor and the boundaries.

4) Azimuthal force distribution: A polar plot of the tangential force is presented in Fig. 9 for a blockage of 19.7 %.

The data presented in the polar plot of Fig. 9 were obtained from a blade perpendicular to a boundary at its initial position ($t = 0$). When the AR is 0.3, the blade is positioned next to one of the closest boundaries at 0°.

A uniform value for the tangential force of 104 kN is observed for the isotropic blockage case (AR = 1). In the wide channel (AR = 0.3), an anisotropic force distribution is obtained due to the interaction of the blade with the boundaries. Higher force values are observed when the blade passes near the boundaries. This is a direct consequence of the interactions discussed in the previous section.

5) Wake development: Fig. 8 illustrates the wake velocity behind the turbine at a fixed aspect ratio of 0.3

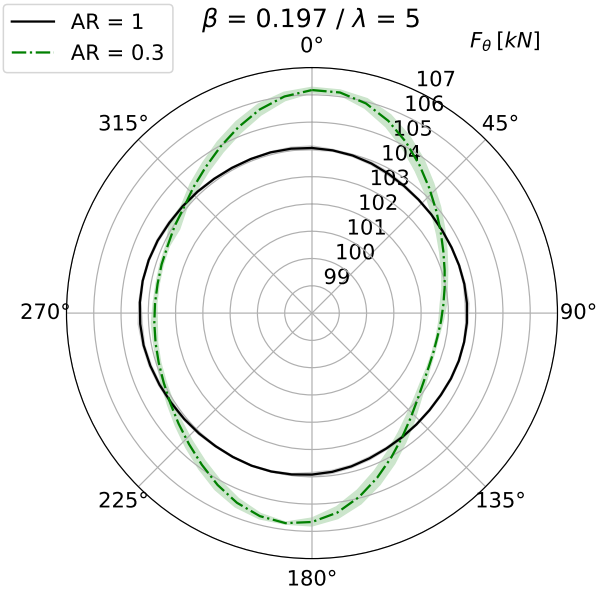

Fig. 9. Angular distribution of the tangential force for two aspect ratios and blockage

and the latest time-step of simulation. In the presence of low isotropic blockage (β = 0.01 and AR = 1), the flow develops symmetrically around the turbine's rotational axis. For the anisotropic blockage, a non-symmetry is observed. In the lower part, the velocity is less signifficant than in the upper part.

Increasing blockage results in a delay in wake recovery. At high blockage, the rotor extracts more power from the incoming flow, removing a larger amount of kinetic energy. In addition, the blocked cases have less energy available for exchange between the wake and the bypass flow due to the boundary confinement. These two effects result in the observed increase in wake length.

Fig. 10 displays the velocity distribution behind the rotor for different aspect ratios at a fixed β of 0.1.

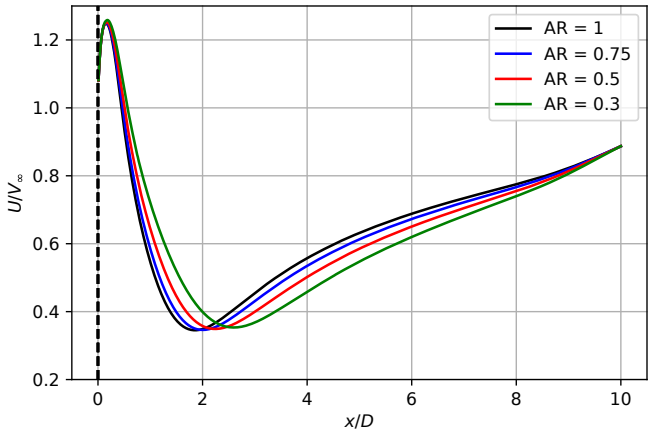

Fig. 10. Axial velocity distribution at the center of the channel (z/D = 0) for different aspect ratios. The blockage is set to 10 % and the rotor is placed at the center of the channel. The vertical black dashed line represents the rotor plane

The sampling was made at the turbine center along the x-axis. As with blockage, aspect ratios also have an

impact on wake development. The distance at which the velocity reaches its lowest values (x/D = 2 at AR = 0.75 for example) increases by 12.5 % when the aspect ratio varies from 1 to 0.3. However, the minimum reach is increasing as the aspect ratio decreases. When the aspect ratio varies from 1 to 0.3, the distance to recover 80 % of the initial velocity increases by 3.93 %.

The velocity distribution for β = 0.01 is presented in Fig 11. In this case, the minimum value is reached at a shorter distance, compared to the $\beta = 0.10$ case. The minimum velocity decreases with the aspect ratio, unlike the cases with higher blockage, and wake recovery is observed to occur faster.

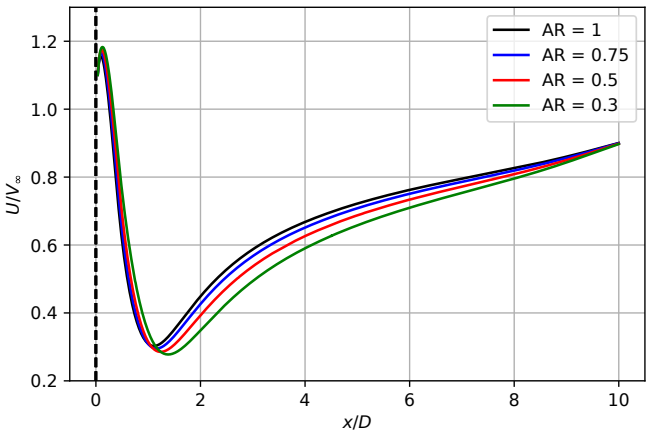

Fig. 11. Axial velocity distribution at the center of the channel (z/D = 0) for different aspect ratios. The blockage is set to 1 % and the rotor is placed at the center of the channel. The vertical black dashed line represents the rotor plane

At low blockage, the wake could potentially exchange more energy with the bypassing flow. This exchange leads to a decrease in the wake length.

This phenomenon could potentially impact multi-turbine operation, where the interactions between adjacent turbines and their wakes could result in further perturbations to the flow field, loads, and power performance. Our results, however, are not conclusive in that regard given the limited scope, and the aspect ratio effects could be investigated for multi-rotor operations as done by, e.g., Nishino and Willden [16].

IV. Conclusion

The effects of blockage on the performance of a turbine have been studied through the analysis of various parameters using the Actuator-Line method. In this study, the simulation domains were defined by rectangular cross-sections of different aspect ratios and global blockages. Our baseline results for isotropic blockage were in agreement with previous studies: an increase in blockage results in higher thrust and power performance. Concerning the anisotropic blockage, the power extracted decreases with lower aspect ratios when blockage approaches zero. At low values of β and aspect ratio, the presence of the turbine has a lower impact on the flow. Reduced performance is observed in this case. When the blockage increases, however, the blades interact with the surrounding boundaries, as shown by, e.g., the polar distribution of tangential force. Under these circumstances, the boundaries affect flow development across the rotor plane and induce changes to the sectional angles of attack. Depending on the analysed cases and region of the blade, angles of attack can increase or decrease, affecting both local and integrated power and thrust.

However, our research also shows that an increase in mean power extraction is possible in some configurations. Rotor farms could be designed to exploit the local bathymetry of a channel, which is likely to have a significant blockage and an aspect ratio below 1. These characteristics have the potential to increase energy yields and reduce the levelized cost of energy.

Regarding the wake development, the velocity profile can be affected by the blockage and the aspect ratio. The wake took a longer distance to recover 80 % of its initial speed ($\approx$ 4%) between the highest and the lowest value of aspect ratio at β = 0.1. This could have significant implications for the design of tidal rotor arrays, affecting the overall performance and efficiency of the system [19]. If the wake is shorter, it may be possible to pack more turbines in a given area, thereby potentially increasing the overall power output.

Through the study, the effect of the aspect ratio has demonstrated low importance compared to global blockage. In the case of low blockage (β = 0.01), the aspect ratio has a diminishing effect on the overall power and thrust generated by the rotor. These are not time-dependent and do not exhibit significant fluctuations. When the blockage is combined with the aspect ratio, and despite the time-averaged values showing similar results to the isotropic case, we could observe significant fluctuations in time. These fluctuations are related to the angle of attack and the axial force along the blade, with a larger range of variations for lower aspect ratios.

The study has been limited to blockage and aspect ratios. Despite the cases with aspect ratios below one resemble realistic tidal channels better than an isotropic blockage, this does not fully capture the complexity of real deployment sites. Futures studies will address more complex bathymetric features.

Acknowledgements

The authors acknowledge the financial support from Normandy Region through the Laboratoire d'Excellence Energy, Materials and Clean Combustion Center (LabEx EMC3) and the Graduate School Materials and Energy Sciences (GS-MES)
This project received funding from the European Union's Horizon 2020 research and innovation programme under the Marie Skłodowska-Curie grant agreement No 101034329, recipient of the WINNING-Normandy Program supported by the Normandy Region.
This work was funded as part of the Tidal Stream Industry Energiser Project (TIGER), a European Union INTERREG V A France (Channel) England Research and Innovation Programme, which is co-financed by the European Regional Development Fund (ERDF).
The present work was performed on computing resources provided by CRIANN (Normandy, France)

REFERENCES

[1] AS Bahaj, AF Molland, JR Chaplin, and WMJ Batten. Power and thrust measurements of marine current turbines under various hydrodynamic flow conditions in a cavitation tunnel and a towing tank. *Renewable energy*, 32(3):407–426, 2007.

[2] Jewel B Barlow, William H Rae, and Alan Pope. *Low-speed wind tunnel testing*. John wiley & sons, 1999.

[3] Chang-Koon Choi and Dae-Kun Kwon. Wind tunnel blockage effects on aerodynamic behavior of bluff body. *Wind Struct Int J*, 1(4):351–364, 1998.

[4] Peter Fuglsang and Kristian S Dahl. Design of the new riso-a1 airfoil family for wind turbines. In *EWEC-CONFERENCE-*, pages 134–137, 1999.

[5] Chris Garrett and Patrick Cummins. The efficiency of a turbine in a tidal channel. *Journal of fluid mechanics*, 588:243–251, 2007.

[6] H Glauert. Wind tunnel interference on0 wings, bodies and airserews 0. 1933.

[7] John J Harper and Alan Pope. Low-speed wind tunnel testing john wiley & sons. *Inc. New York, NY*, 1966.

[8] Eva Jost, Levin Klein, Hagen Leipprand, Thorsten Lutz, and Ewald Krämer. Extracting the angle of attack on rotor blades from cfd simulations. *Wind Energy*, 21(10):807–822, 2018.

[9] Marcus CR Juniper and Takafumi Nishino. A data-informed analytic model for turbine power prediction with anisotropic local blockage effects. In *Journal of Physics: Conference Series*, volume 2265, page 022046. IOP Publishing, 2022.

[10] EC Maskell. A theory of the blockage effects on bluff bodies and stalled wings in a closed wind tunnel. Technical report, Aeronautical Research Council London (United Kingdom), 1963.

[11] GN McCann. Tidal current turbine fatigue loading sensitivity to waves and turbulence–a parametric study. In *Proceedings of the 7th European Wave and Tidal Energy Conference*, 2007.

[12] Florian R Menter. Zonal two equation $k-\omega$ turbulence models for aerodynamic flows. In *23rd fluid dynamics, plasmadynamics, and lasers conference*, page 2906, 1993.

[13] Florian R Menter, Martin Kuntz, and Robin Langtry. Ten years of industrial experience with the sst turbulence model. *Turbulence, heat and mass transfer*, 4(1):625–632, 2003.

[14] R Mikkelsen and JN Sørensen. Modelling of wind turbine blockage. In *15th IEA symposium on the aerodynamics of wind turbines, FOI Swedish Defence Research Agency*, 2002.

[15] Karl Nilsson, Wen Z Shen, Jens N Sørensen, Simon-Philippe Breton, and Stefan Ivanell. Validation of the actuator line method using near wake measurements of the mexico rotor. *Wind Energy*, 18(3):499–514, 2015.

[16] Takafumi Nishino and Richard HJ Willden. Effects of 3-d channel blockage and turbulent wake mixing on the limit of power extraction by tidal turbines. *International Journal of Heat and Fluid Flow*, 37:123–135, 2012.

[17] Patrick J Roache. Quantification of uncertainty in computational fluid dynamics. *Annual review of fluid Mechanics*, 29(1):123–160, 1997.

[18] J Schluntz and RHJ Willden. The effect of blockage on tidal turbine rotor design and performance. *Renewable Energy*, 81:432–441, 2015.

[19] Rabia Shakoor, Mohammad Yusri Hassan, Abdur Raheem, and Yuan-Kang Wu. Wake effect modeling: A review of wind farm layout optimization using jensen s model. *Renewable and Sustainable Energy Reviews*, 58:1048–1059, 2016.

[20] Wen Zhong Shen, Wei Jun Zhu, and Jens Nørkær Sørensen. Actuator line/navier–stokes computations for the mexico rotor: comparison with detailed measurements. *Wind energy*, 15(5):811–825, 2012.

[21] Jens Norkær Sorensen and Wen Zhong Shen. Numerical modeling of wind turbine wakes. *J. Fluids Eng.*, 124(2):393–399, 2002.

[22] Aidan Wimshurst and Richard H. J. Willden. Computational analysis of blockage designed tidal turbine rotors. *Progress in Renewable Energies Offshore - Proceedings of 2nd International Conference on Renewable Energies Offshore, RENEW 2016*, (Emec): 587–597, 2016.

[23] Markella Zormpa, Federico Zilic de Arcos, Xiaosheng Chen, Christopher R. Vogel, and Richard H. J. Willden. The effect of flow sampling on the robustness of the actuator line method. *Wind Energy*, 2023. Submitted.